The role of the land-surface model for climate change projections over the Iberian Peninsula

S. Jerez,[1,2] J. P. Montavez,[1] J. J. Gomez-Navarro,[1] P. A. Jimenez,[3] P. Jimenez-Guerrero,[1] R. Lorente,[1] and J. F. Gonzalez-Rouco[4]

[1] The importance of land-surface processes within Regional Climate Models for accurately reproducing the present-day climate is well known. However, their role when projecting future climate is still poorly reported. Hence, this work assesses the influence of the land-surface processes, particularly the contribution of soil moisture, when projecting future changes for temperature, precipitation and wind over a complex area as the Iberian Peninsula, which, in addition, shows great sensitivity to climate change. The main signals are found for the summer season, when the results indicate a strengthening in the increases projected for both mean temperature and temperature variability as a consequence of the future intensification of the positive soil moisture-temperature feedback. The more severe warming over the inner dry Iberian Peninsula further implies an intensification of the Iberian thermal low and, thus, of the cyclonic circulation. Furthermore, the land-atmosphere coupling leads to the projection of a wider future daily temperature range, since maximum temperatures are more affected than minima, a feature absent in non-coupled simulations. Regarding variability, the areas where the land-atmosphere coupling introduces larger changes are those where the reduction in the soil moisture content is more dramatic in future simulations, i.e., the so-called transitional zones. As regards precipitation, weaker positive signals for convective precipitation and more intense negative signals for non-convective precipitation are obtained as a result of the soil moisture-atmosphere interactions. These results highlight the crucial contribution of soil moisture to climate change projections and suggest its plausible key role for future projections of extreme events.

1. Introduction

[2] Land-surface models (LSMs) arouse a growing interest among climate modelers [*Gulden et al.*, 2008] and large efforts have been made since the first implicit approach representing surface energy balance and hydrology [*Manabe*, 1969] toward attaining a more realistic modeling of the processes through which the land surface influences the climate [*Pitman*, 2003]. *Seneviratne et al.* [2010] offers a wide and updated review on how such complex schemes help us to understand climate variability when used within climate models, overcoming, to some extent, the lack of observational data, particularly regarding soil variables [*Robock et al.*, 2000]. This review highlights the fact that soil moisture is a main land-surface parameter affecting the sub-seasonal to seasonal variability of the atmosphere, providing, in conjunction with soil temperature, a long-term memory factor for the surface boundary condition [*Koster and Suarez*, 2001; *Seneviratne et al.*, 2006a]. Especially in regions where soil moisture can vary seasonally and interannually between dry and wet conditions (the so-called transitional climate zones), as in the Iberian Peninsula (IP), soil moisture will be an important factor influencing the climate due to its control over evapotranspiration and thus over the partitioning of net surface energy into the latent and sensible heat fluxes [*Sridhar et al.*, 2002; *Jaeger et al.*, 2009; *Jerez et al.*, 2010].

[3] Despite the significant divergence between LSMs regarding their performance in climate simulations [*Kato et al.*, 2007], which shows the need for further sensitivity studies aimed at better understanding land surface processes, some basic common interaction mechanisms between land and atmosphere can be identified from multimodel studies such as PILPS [*Henderson-Sellers et al.*, 1996], GLACE [*Koster et al.*, 2004, 2006; *Guo et al.*, 2006], GSWP [*Dirmeyer et al.*, 2006] and LUCID [*Pitman et al.*, 2009].

[1]Departamento de Fisica, Universidad de Murcia, Murcia, Spain.
[2]IDL, Universidade de Lisboa, Lisbon, Portugal.
[3]National Center for Atmospheric Research, Boulder, Colorado, USA.
[4]Departamento Astrofisica y Ciencias de la Atmosfera, Facultad Ciencias Fisicas, Universidad Complutense de Madrid, Madrid, Spain.

For example, the GLACE experiment investigated soil moisture-atmosphere coupling in 12 Atmosphere–ocean General Circulation Models. The geographical hot spot identified, common in all the simulations, were found to be located in transitional zones between wet and dry climates. However, there is still significant uncertainty regarding the precise geographical definition of transitional climate zones and the exact strength of soil moisture-evapotranspiration coupling and its effects on the atmospheric variables.

[4] As regards to near-surface air temperature, substantial evidence exists of the influence of the soil moisture forcing. *Seneviratne et al.* [2006b] and *Fischer and Schär* [2009] showed the relationship between the enhancement of summer temperature variability predicted for Europe and the soil moisture-temperature feedback. *Ferranti and Viterbo* [2006], *Fischer et al.* [2007] and *Jaeger and Seneviratne* [2010] demonstrated the large impact of the soil forcing on both the strength and duration of heat wave events, particularly with regard to daily maximum temperatures. The asymmetric effect on maximum and minimum temperatures and its involvement in the daily temperature range have been particularly highlighted by *Miao et al.* [2007] and *Zhang et al.* [2009]. *Jaeger and Seneviratne* [2010] linked the drying trend observed in the soil moisture series to the mean temperature trends of the recent past, emphasizing the soil moisture amplifying effect. *Jerez et al.* [2010], the closest precedent to the present study, showed that land-atmosphere coupling affects both the annual cycle and the intra and interannual variability of the temperature series when simulating the observed climatology of the IP, reducing underestimation of both the mean values and the variability of the temperature series and improving the representation of the spatial heterogeneities of the temperature patterns.

[5] However, the role of soil moisture for forecasting precipitation is not as clear as it is in the case of temperature, since the interactions are not as straightforward [*Seneviratne et al.*, 2010]. Indeed, despite many works dealing with this topic [*Betts*, 2004; *Koster et al.*, 2004; *Luo et al.*, 2007; *Taylor et al.*, 2007; *Yang et al.*, 2007; *Alfieri et al.*, 2008; *Hohenegger et al.*, 2008; *Zhang et al.*, 2008; *Steiner et al.*, 2009], substantial uncertainties still remain. It is still unclear whether, how and under what circumstances, soil-atmosphere interactions may influence precipitation forecasts; although most studies agree that the most affected areas show semihumid conditions and strong hydroclimatic gradients, as do some regions of the IP. Moreover, there is a lack of knowledge about the soil moisture contribution to future projections for precipitation.

[6] Not only temperature and precipitation but also other atmospheric variables can be greatly affected by the soil forcing, specifically soil moisture forcing, such as surface wind. Nonetheless, our understanding of the soil moisture influence on the surface circulation is even more limited than over precipitation. Only a few studies have investigated the influence of this kind of land-atmosphere feedback [*Haarsma et al.*, 2009; *Jimenez et al.*, 2011].

[7] Moreover, it must be expected that the location and/or intensity of the soil moisture-climate interactions inferred from present period simulations or observations will not hold under future enhanced greenhouse gas concentrations. For instance, shifts in climate regimes may modify the location of transitional climate zones.

[8] These considerations motivated us to explore the role of the land-surface model in regional climate simulations performed for the Iberian Peninsula aimed at projecting future changes in seasonal mean values and temporal variability of temperature, precipitation and surface wind, for both winter and summer seasons. The procedure involves the comparison of analogous simulations performed with different LSMs in order to isolate climate change signals attributable to the forcing resulting from land-surface processes. Special attention is paid to the soil moisture contribution, although the experiments were not designed to specifically filter its contribution.

[9] Given the lack of studies dealing with the sensitivity of RCM simulations to the land-surface model at climatic scales, this work presents novelties and a valuable information, particularly regarding the IP. Moreover, the IP is an excellent region for the specific purposes of the present investigation. On the one hand the IP presents a strong spatial and temporal climate heterogeneity. Such heterogeneity stems from the interaction of the large-scale flow and the complex topography. It ranges from the Mediterranean climate, characterized by warm and dry summers with convective-predominant precipitation and cold humid winters with large-scale induced precipitation, to milder winters and wetter summers toward the north and west mainly connected to large-scale synoptic systems including the North Atlantic Oscillation [*Sumner et al.*, 1995; *Font-Tullot*, 2000; *Gonzalez-Rouco et al.*, 2000]. Hence, the analysis can be made under diverse conditions. On the other hand, the IP, as part of the Mediterranean region, has been identified as one of the regions of the world most likely to be affected by climate change [*Giorgi*, 2006]. Robust signals of increase in mean temperature, temperature variability and precipitation variability, and decrease in mean precipitation are projected especially for the dry and warm season (although a few exceptions add some controversy in the case of the precipitation projections), as well as more frequent and persistent heat waves [e.g., *Gallardo et al.*, 2001; *Trigo and Palutikof*, 2001; *Giorgi*, 2006; *Christensen and Christensen*, 2007; *Tapiador et al.*, 2007; *Della-Marta et al.*, 2007; *May*, 2008; *Fischer and Schär*, 2009; *Gomez-Navarro et al.*, 2011]. In addition, a plausible depletion of the soil moisture content in a warmer future scenario would turn some currently wet areas of the IP into semiarid regions [*Gao and Giorgi*, 2008]. In such a scenario, shifts and/or widenings of the areas that show a strong response to the soil moisture forcing, and an intensification of the soil moisture-temperature feedback within them, are to be expected [*Jerez et al.*, 2010; *Jaeger and Seneviratne*, 2010; *Seneviratne et al.*, 2010]. Thus, a thorough evaluation of the mechanisms contributing to climate changes in this particular area results of general relevance.

[10] This work is structured as follows. Section 2 describes the numerical experiments. Section 3 presents and discusses the results and Section 4 summarizes and highlights the main conclusions.

2. Experimental Design

[11] Four regional climate simulations were performed with a climate version of the mesoscale model MM5 [*Grell et al.*, 1994], which allows to use the same external
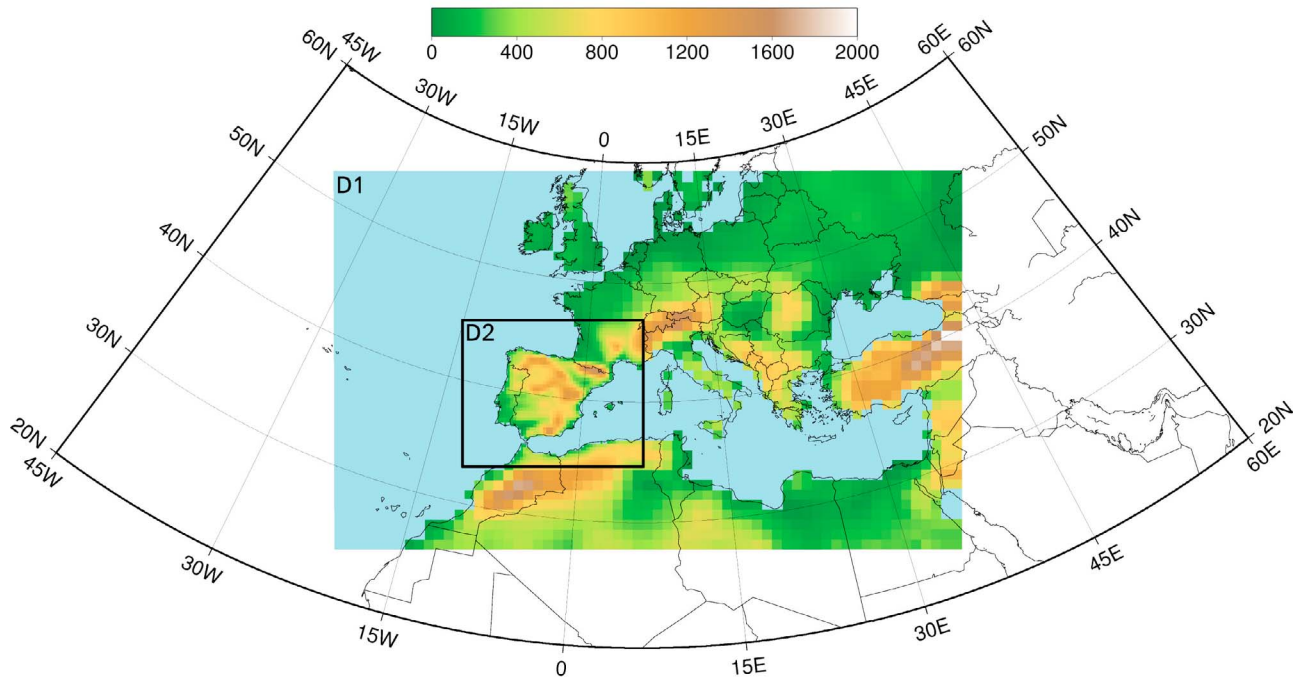
Figure 1. Domains configuration used in the MM5 simulations. Shaded colors depict the orography seen by the model (terrain height, in m) at the corresponding spatial resolutions: 90 km (D1) and 30 km (D2). Water masses (seas and oceans) are plotted in light blue.

forcings (i.e. the GHGs and aerosol concentrations) in both the regional simulation and the global simulation driving it. MM5 has been widely used in many previous works [e.g., *Fernandez et al.*, 2007; *Koo et al.*, 2009; *Jimenez-Guerrero et al.*, 2010; *Gomez-Navarro et al.*, 2010] and its accuracy when simulating mesoscale circulations and reproducing regional climates is widely accepted [e.g., *Kanamitsu et al.*, 2002; *Gomez-Navarro et al.*, 2011; *Jerez et al.*, 2010].

[12] The simulations span the intervals 1961–1990, as the control reference period (CTRL), and 2070–2099, to describe a climate change scenario simulation (SCEN), and have been driven by outputs from the ECHO-G Global Circulation Model. For the scenario period, the extension of the ECHO-G run under the SRES A2 scenario is considered. See *Legutke and Voss* [1999] for details of the ECHO-G model and *Zorita et al.* [2005] for details of the ECHO-G simulation used in this work. The difference between the climatology simulated for the future period and the climatology reproduced for the present period will depict the projected changes assessed below.

[13] Both the CTRL and the SCEN simulations have been performed twice, first using the Noah Land Surface model (NOAH) [*Chen and Dudhia*, 2001] and secondly using the Simple Five-Layer soil model (SLAB) [*Dudhia*, 1996]. Thus, the contribution of the land-surface processes will be depicted by comparing the SLAB and NOAH simulations. Both schemes use the same formulation and the main difference between them lies in the treatment of soil moisture, although other important parameters that may play important roles, such as vegetation and soil layer depths, are also

differently represented (refer to *Jerez et al.* [2010] for details). In the SLAB simulations, soil moisture availability is fixed to climatological values which simply depend on the land use category of each grid cell and do not change during the simulated period. Conversely, in the NOAH simulations, available soil moisture and the soil thermal state change according to processes such as evapotranspiration, water intercepted by the canopy, root absorption of water, surface runoff and subsurface drainage.

[14] The ability of MM5 using NOAH and SLAB to reproduce a realistic temperature climatology for the IP when driven by the ERA40 reanalysis was evaluated by *Jerez et al.* [2010]. The results showed that, although computationally more expensive, the use of the NOAH scheme improves the accuracy of the simulation, especially in summer for the driest areas of the IP. However, that study did not explore precipitation, but, as demonstrated by *Gomez-Navarro et al.* [2010], we are also confident concerning the reliability of the couple MM5+NOAH in this regard.

[15] Spatial and physical configurations of the model are common for all the simulations. The spatial set up consists of two two-way nested domains with spatial resolutions of 90 and 30 km (Figure 1). The inner domain covers the full IP even after excluding the 5 outermost grid points which were affected by the relaxation to the outer domain. This outer domain is displaced eastward in order to include the strong influence that the Mediterranean Sea exercises over the IP. The physical parameterizations used are: Grell cumulus parameterization [*Grell*, 1993], Simple Ice for microphysics [*Dudhia*, 1989], MRF for the planetary boundary layer
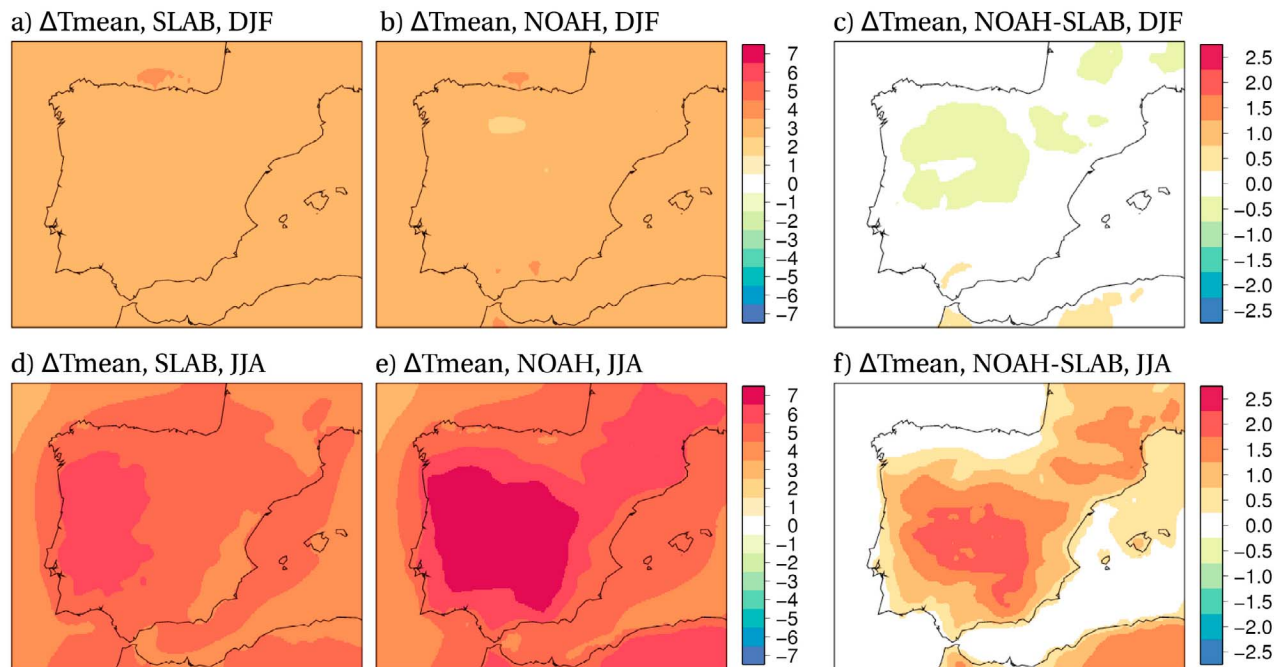
Figure 2. (a, b, d, and e) Projections for mean temperature (Tmean), using either the SLAB or the NOAH scheme, for the winter (DJF) and summer (JJA) seasons. (c and f) The differences between the NOAH and the SLAB projection. Units: K.

[*Hong and Pan*, 1996] and the RRTM radiation scheme [*Mlawer et al.*, 1997]. The 30-year-long simulations were performed by continuous runs of 5-year length with a previous spin-up period of 4 months, which is discarded in the analysis to prevent the initial noise of the outputs (when the model is still stabilizing) and the undesirable influence of a possible poor initialization. Outputs for the IP were recorded every 6 hours.

3. Results and Discussion

[16] The analysis focuses on mean values and interannual variability of seasonal averages of temperature (T), precipitation (P) and wind. The units of precipitation are mm/month because the seasonal averages are computed from monthly series, but we just retain one seasonal record per year. Interannual variability is characterized by the standard deviation of the detrended series (sdev). Spring (MAM) and autumn (SON) were found to show intermediate behavior between winter (DJF) and summer (JJA) seasons. Thus, we focus on these two seasons for the sake of clarity and brevity. Temperature projections are analyzed in the next section, precipitation projection are analyzed in Section 3.2 and the most important characteristic of the wind projections in Section 3.3.
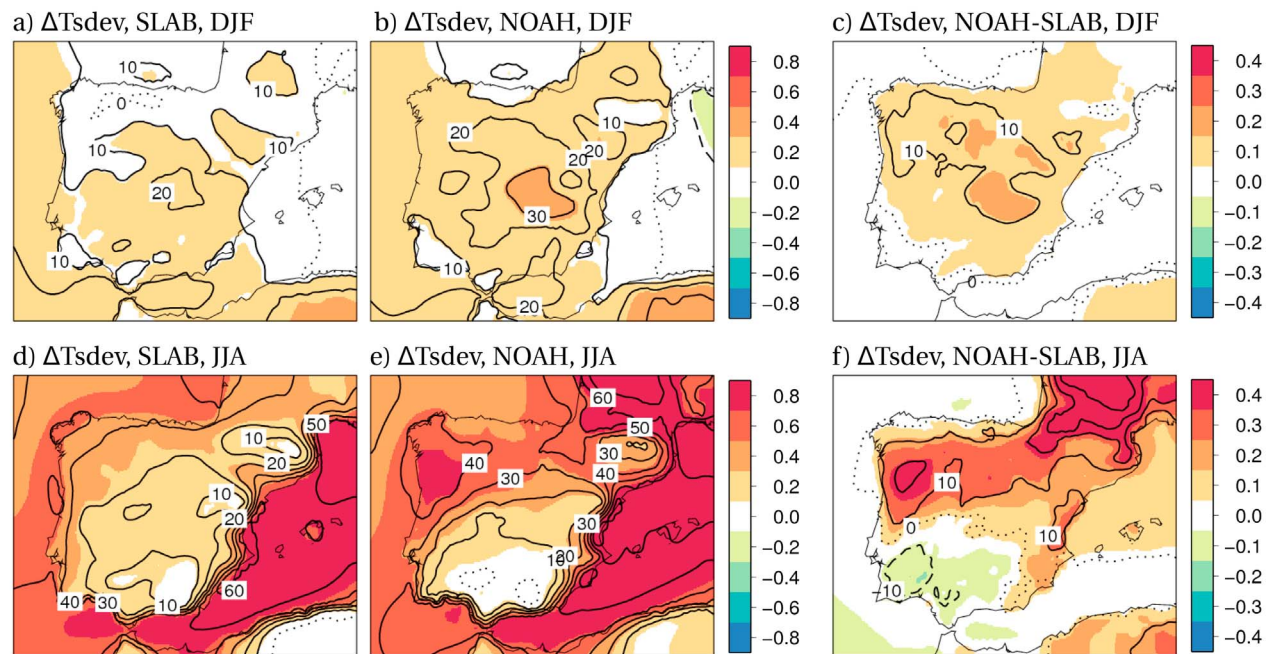
3.1. Temperature Projections

[17] Figure 2 shows the mean temperature change projections for winter and summer when using each LSM, and the differences between the NOAH and SLAB projections. In winter, warming patterns do not differ much, present homogeneous spatial structure and project increases of around 3 K. In the summer season, changes are more pronounced inland and toward the west of the IP, reaching values up to 7 K in the NOAH simulation, up to 2 K higher than those projected by the SLAB simulation. Furthermore, these notable differences between the NOAH and SLAB simulations affect the areas where changes are most pronounced.

[18] The interannual variability of the temperature series (Tsdev) is also projected to increase everywhere and in every season (Figure 3). In winter, the projected increase is around 0.2 K (∼20%) and fairly homogeneous over the entire domain (Figures 3a and 3b). Differences between SLAB and NOAH are around 0.1 K. The NOAH simulation projects an increase about 15% greater over the northern and inner areas of the IP than the SLAB simulation (Figure 3c). In the summer season (Figures 3d and 3e), the projected changes are again larger than in the winter season, showing the largest signals over water mass areas, especially over the Mediterranean Sea (over 0.8 K, ∼ over 50%), followed by the northern land areas of the IP (where changes are around 0.6–0.8 K, ∼ up to 50%). Substantial differences appear between the SLAB and NOAH projections inland, depicting a north–south gradient (Figure 3f). NOAH projects much greater increase in the temperature variability in the northern IP, where changes are most pronounced; the differences between both projections being more than 0.4 K (20%). Conversely, in the south-western IP the SLAB model leads to a larger increase of the variability (up to 15%).

[19] It was to be expected that differences between NOAH and SLAB could mainly affect the summer season, as seen above, for two reasons. On the one hand, large scale circulation strongly drives temperature in winter, while in summer the synoptic scale winds are weaker and local circulations become more relevant in midlatitude regions

Figure 3. (a, b, d, and e) Projections for the interannual variability of the temperature series (Tsdev), using either the SLAB or the NOAH scheme, for the winter (DJF) and summer (JJA) seasons. (c and f) The differences between the NOAH and the SLAB projection. Units: K in shading. Contours depict changes in percentage with respect to the reference period in Figures 3a, 3b, 3d and 3e; and differences between NOAH and SLAB in the changes expressed in percentage in Figures 3c and 3f. Solid contours are positive, dashed contours are negative, and dotted contours represent zero-isolines. Contour interval is 10.

such as the IP. On the other hand, solar forcing is weaker in winter than in summer and, therefore, less heat is available for the partitioning into sensible and latent fluxes (which greatly determines the assessed LSM-impact, as shown below). Both features prevent a strong influence of in-situ processes, such as soil-atmosphere feedbacks, in the winter season, while emphasizing the importance of the LSM in the summer season.

[20] Of note is the fact that the LSM-impact patterns show the strongest signals in areas where the projected changes are larger. That is, the hot spot areas/seasons are very sensitive to the LSM. Hence, the underlying mechanisms are worth investigating for a deeper understanding of potential risks. In order to attribute causes for the main differences between the SLAB and NOAH projections, an analysis of the soil energy and moisture budget was performed, and impacts on maximum and minimum temperatures (TX and TN, respectively) were investigated.

[21] Figure 4 shows the mean soil moisture content (available water for evapotranspiration) simulated by NOAH for the present and future periods and the differences between them. The difference in the way soil moisture availability is treated by the SLAB scheme prevents a direct comparison with the NOAH simulation in this regard. Nonetheless, it is clear from these plots that the LSM-impact pattern for the summertime mean temperature projection (Figure 2f) shows the strongest signals over some of the driest areas of the IP, the inner ones not greatly affected by
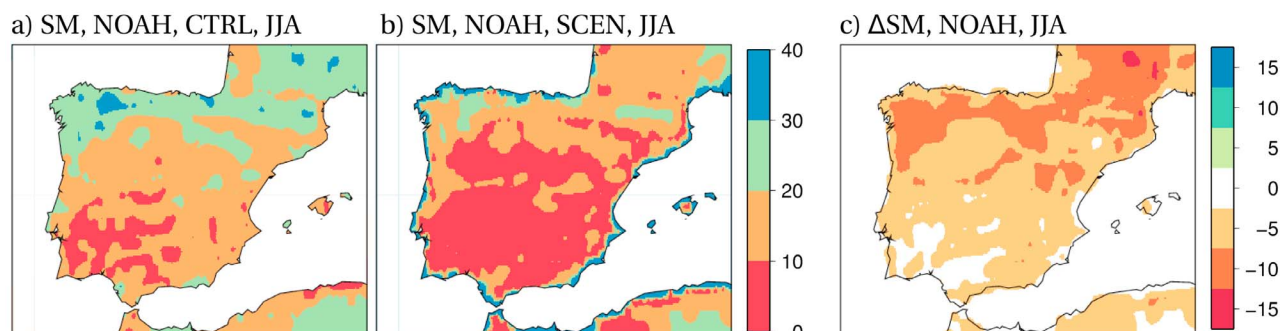
Figure 4. Simulated soil moisture - saturation level in the first 1m-soil layer. (a and b) Climatologies reproduced by the NOAH simulation in the CTRL and SCEN periods for the summer (JJA) season. (c) Future projection (SCEN minus CTRL). Units: %.

a) SH, NOAH-SLAB, CTRL, JJA b) SH, NOAH-SLAB, SCEN, JJA c) ΔSH, NOAH-SLAB, JJA
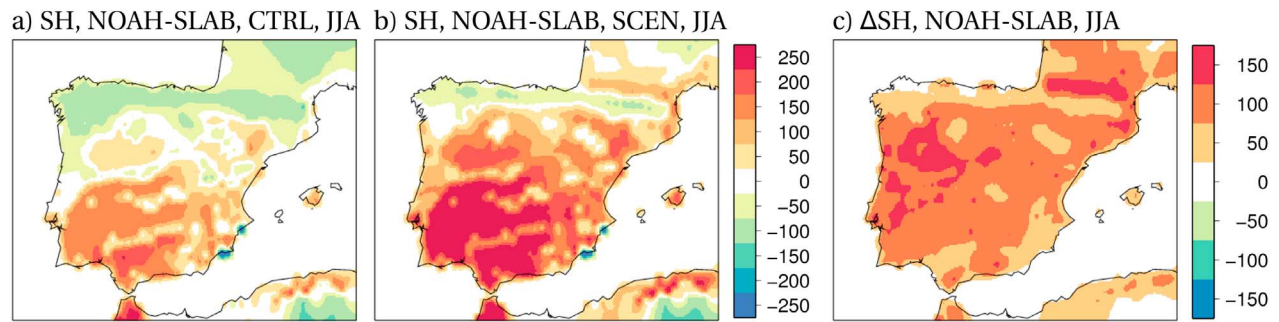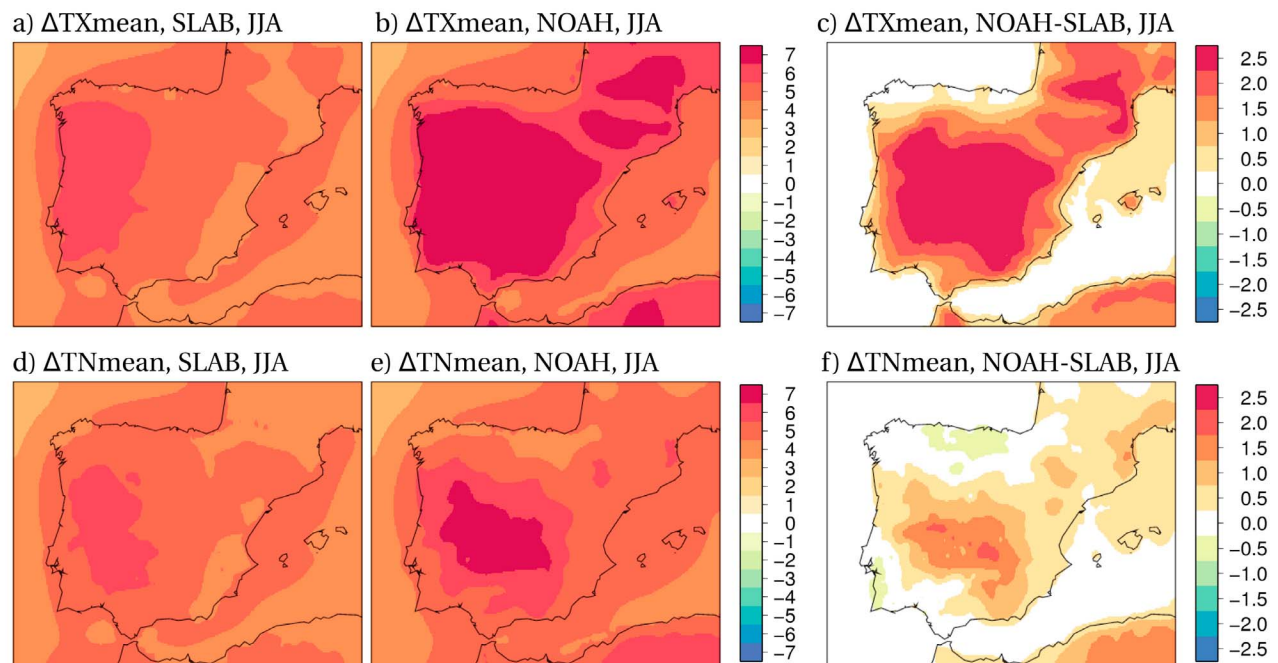

Figure 5. Simulated daily maximum surface sensible heat flux. (a and b) Differences between the NOAH and the SLAB simulation (NOAH minus SLAB) in the climatologies reproduced in the CTRL and SCEN periods for the summer (JJA) season. (c) Differences between the NOAH and SLAB simulations (NOAH minus SLAB) in the future projections (SCEN minus CTRL). Units: W/m^2.
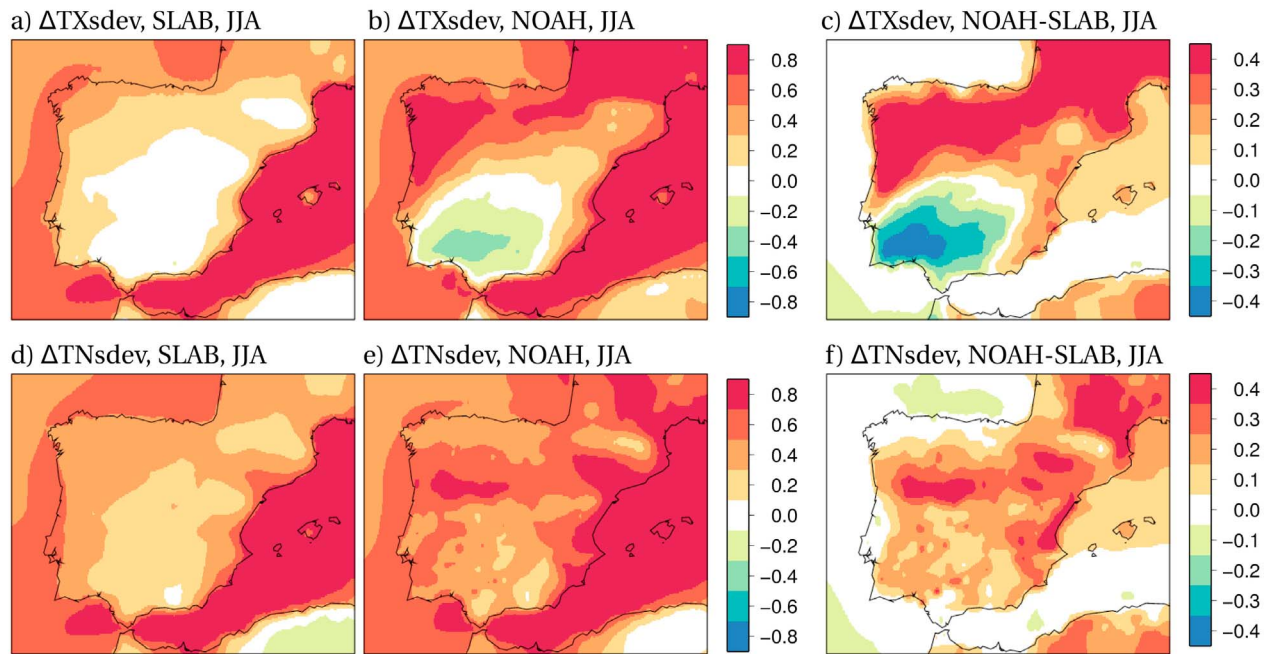
advection phenomena from the ocean (Figures 4a and 4b). The main cause is related to the larger surface sensible heat flux (SH) simulated when the NOAH scheme is used (Figure 5) at the expense of the latent heat flux (differences in the rest of the terms involved in the surface energy balance equation are some orders of magnitude smaller, not shown). The patterns of differences in the simulated SH match those of the soil moisture content obtained from the NOAH simulations. Bearing in mind that the values of soil moisture availability used by the SLAB model do not vary much between regions because of the vast land use assignment (not shown), and given that the future depletion of the soil moisture availability projected by the NOAH simulations is accompanied by a future intensification of the differences between NOAH and SLAB in the simulated SH (in favor of NOAH) (Figures 4a and 5a versus Figures 4b and 5b), the

results support that the main cause for the differences in the temperature projections would lie in the future intensification of a positive soil moisture-temperature feedback (Figure 5c) which is simulated when the NOAH scheme is used but is avoided in the SLAB simulations. The feedback is as follows: the less soil moisture available, the less latent heat flux and hence the larger the sensible flux released (differences between NOAH and SLAB reach midday values of around 200 W/m^2 in vast areas of the IP, Figure 5b), which originates higher temperatures, and so on. Such a soil moisture-amplifying effect is hidden in the SLAB simulation, which treats soil moisture as a static field. Although strong in most of the IP, land-sea breezes smooth this effect near the sea.

[22] The analysis of the daily mean summertime TX and TN projections (Figure 6) points to a greater LSM-impact on TX (more than 2.5 K over wide inner areas) than on TN,

a) ΔTXmean, SLAB, JJA b) ΔTXmean, NOAH, JJA c) ΔTXmean, NOAH-SLAB, JJA

d) ΔTNmean, SLAB, JJA e) ΔTNmean, NOAH, JJA f) ΔTNmean, NOAH-SLAB, JJA

Figure 6. (a, b, d, and e) Projections for summer (JJA) mean daily maximum (TX; upper) and daily minimum (TN; bottom) temperature when using either the SLAB or the NOAH scheme. (c and f) The differences between the NOAH and the SLAB projection. Units: K.

a) ΔTXsdev, SLAB, JJA   b) ΔTXsdev, NOAH, JJA   c) ΔTXsdev, NOAH-SLAB, JJA

d) ΔTNsdev, SLAB, JJA   e) ΔTNsdev, NOAH, JJA   f) ΔTNsdev, NOAH-SLAB, JJA

Figure 7. (a, b, d, and e) Projections for summertime (JJA) interannual variability of mean daily maximum (TX; upper) and daily minimum (TN; bottom) temperature series when using either the SLAB or the NOAH scheme. (c and f) The differences between the NOAH and the SLAB projection. Units: K.

which further supports the above argument. The positive soil moisture-temperature feedback is stronger at daytime, i.e. the upward flux of sensible heat from the warm soil to the upper atmosphere is larger at daytime than at nighttime, when indeed the soil becomes cooler than the atmosphere as the solar radiation ceases. Such feedback involves a reduction of the soil moisture availability, which, in turn, reduces both, the latent heat released from evapotranspiration processes (in favor of the exchange of sensible heat), and the soil heat capacity in comparison with moister soils (which leads to even warmer soils). However, even though such a reduction in the soil heat capacity due to the depletion of soil moisture speeds the soil cooling process at night, the NOAH projection for TN is still greater than the SLAB projection (Figure 6f). The reason seems to be associated with the large amount of heat stored in the ground during daytime, which presumably counteracts the faster radiative cooling process (at nighttime) as the soil dries.

[23] The former assessment of TX and TN projections reveals an additional interesting feature. In the NOAH simulations, TX is foreseen to increase more than TN over the whole IP, a behavior which is totally masked in the SLAB simulations. Such asymmetry, already reported by *Gomez-Navarro et al.* [2010], involves a wider daily temperature range and highlights the importance that the LSM may have for accurately projecting extreme temperatures.

[24] The role of the LSM as regards the interannual variability in temperatures is more complex and confined to the so-called transitional climate zones, defined as those changeable between wet and dry regimes. Figure 4c shows that the northern IP is greatly affected by future depletion of the soil moisture content in the summer, which would turn these currently wet areas into semiarid ones. On the other hand, the LSM-impact pattern regarding summertime temperature

variability is stronger in these areas. As other authors have found over various domains [e.g., *Seneviratne et al.*, 2006b], such a transition from wet to dry conditions effectively enhances the former projections for Tsdev.

[25] Note that the differences between NOAH and SLAB as regards the interannual variability of the mean summer temperatures are mainly due to differences in the interannual variability of the TX series while differences in TN are much smaller (Figure 7). As discussed above, the role of the LSM is more noticeable during daytime. Besides, Figure 7 clearly yields another interesting result in line with the above attribution: the reduction of the interannual variability of TX projected by the NOAH simulations over the southern IP. This area shifts from a transitional regime to a fully dry one and becomes so dry in the NOAH simulation during the SCEN period (Figure 4b) that the rainfall events can not notably modify the absence of available soil moisture. Thus, soil conditions remain quite constant with time without influencing the temperature variability. Conversely, the still transitional regime of the southern IP in the CTRL period allows for larger soil moisture variability and thus a larger temperature variability than in the SCEN period.

3.2. Precipitation Projections

[26] Precipitation is, in general, projected to decrease by both experiments in all seasons (Figures 8a, 8b, 8d, and 8e). The largest reduction affects a vast extension of the western IP in winter (above 50 mm/month), followed by the northern IP in summer (up to 40 mm/month). These large signals affect some of the rainiest areas. Hence, when the changes are expressed as a percentage, the signals are shifted southward in winter and westward in summer, in both cases up to 70%. Differences between NOAH and SLAB projections for mean precipitation are slight in the winter, but not in the
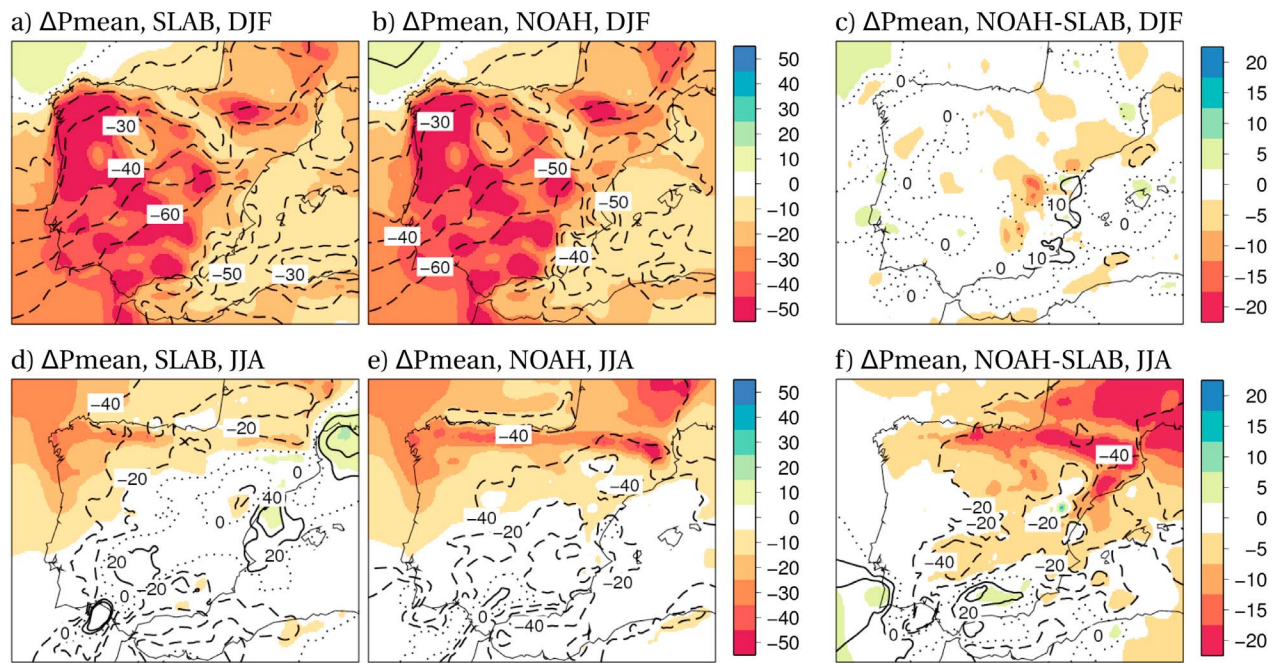
Figure 8. (a, b, d, and e) Projections for mean precipitation (Pmean), using either the SLAB or the NOAH scheme, for the winter (DJF) and summer (JJA) seasons. (c and f) The differences between the NOAH and the SLAB projection. Units: mm/month. Contours depict changes in percentage with respect to the reference period in Figures 8a, 8b, 8d and 8e; and differences between NOAH and SLAB in the changes expressed in percentage in Figures 8c and 8f. Solid contours are positive, dashed contours are negative, and dotted contours represent zero-isolines. Contour interval is 10 (Figures 8a–8c) and 20 (Figures 8d–8f).

summer, when NOAH enhances the projected reduction in precipitation by up to 20 mm/month over the Pyrenees (Figures 8c and 8f). Differences between both projections when expressed as a percentage range from 20 to 40%.

[27] Regarding the standard deviation of the precipitation series (Psdev), the projections show a decrease in winter over most of the IP (over 20 mm/month) except for the northern IP (Figures 9a and 9b). Thus the extreme precipitation events are projected to increase there, since mean precipitation is projected to decrease while precipitation variability is predicted to increase. As for mean precipitation, the signals are shifted southward when changes are expressed as a percentage. They grow above 40%. In the summer season, the change patterns do not show a clear structure, alternating positive and negative signals (both above 20 mm/month, above 60%); the former mainly over the Mediterranean Sea and the latter mainly over the western IP (Figures 9d and 9e). Differences between the SLAB and the NOAH projections are again larger for summer than for winter (Figures 9c and 9f) and show a quite noisy pattern, with values ranging from −20 to 20 mm/month, which makes it difficult to draw general conclusions but, at the same time, reveals the strong influence of the soil processes.

[28] As for temperature, the former results highlight that the contribution of the LSM has more weight during the summer season. It can also be drawn that, although the main projected changes are imposed by the boundary conditions, the LSM plays a fundamental role in modifying (enhancing or smoothing) the general structure of the climate change patterns, and thus deserves large attention.

[29] To better understand the above results we looked separately at the convective and non-convective components of precipitation. We also looked at the change signals for the frequency and intensity of the rainfall events, which provided more valuable information than the assessment of variability (since the latter is closely tied to the precipitation amount over the IP). Figures 10 and 11 depict this information.

[30] In winter, the convective precipitation is almost negligible while in summer it accounts for over 40% of the total amount of precipitation in some inner and southern areas. This is quite similar in both NOAH and SLAB simulations (not shown). Future changes are projected for both components. In winter, signals come basically from non-convective precipitation and there is no large influence of the LSM (not shown). Conversely, in the summer season, changes in both convective and non-convective precipitation contribute to the projected changes in the total amount of precipitation. Moreover, these two contributions depict opposite signs. Convective precipitation is projected to increase in northeastern areas (about 10 mm/month, Figures 10a and 10b), while non-convective precipitation is projected to decrease in the northern IP (up to 50 mm/month over the Pyrenees, Figures 11a and 11b). Although the change patterns depict similar structures whether the SLAB or the NOAH scheme is used, the signals show different intensities depending on the LSM choice. The LSM-impact patterns highlight that the positive signals for convective precipitation are strengthened when the SLAB scheme is used, while the negative signals of non-convective precipitation are more intense when the
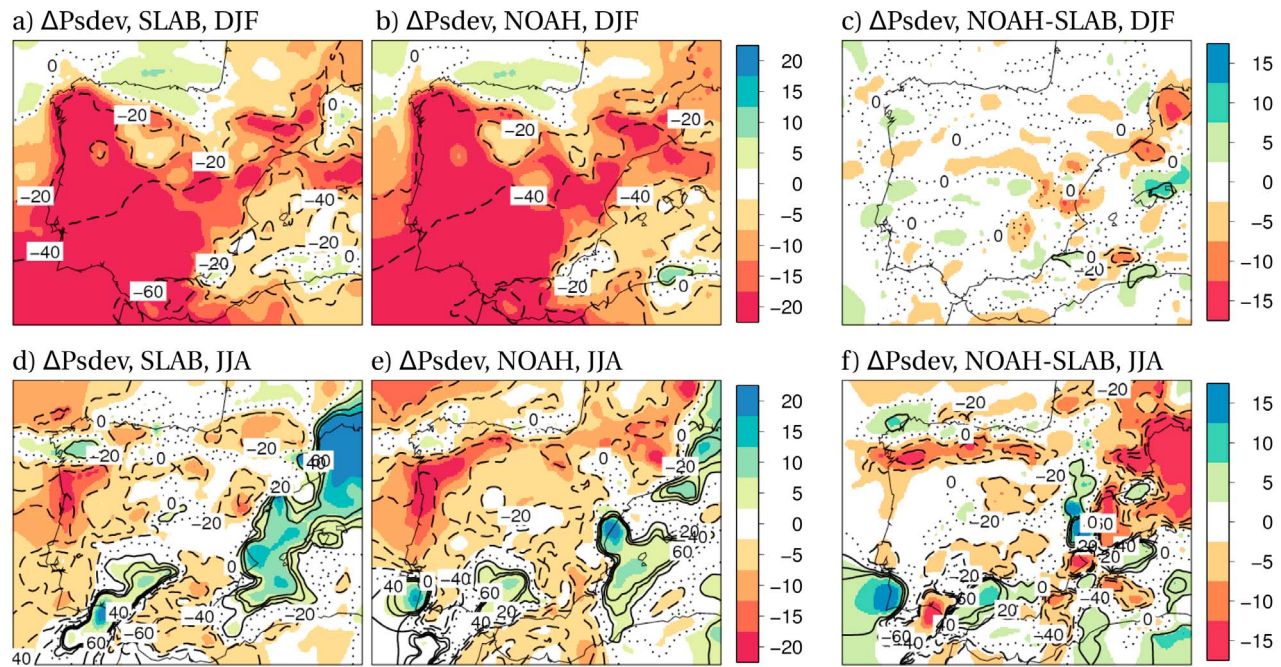
Figure 9. (a, b, d, and e) Projections for the interannual variability of the precipitation series (Psdev), using either the SLAB or the NOAH scheme, for the winter (DJF) and summer (JJA) seasons. (c and f) The differences between the NOAH and the SLAB projection. Units: mm/month. Contours depict changes in percentage with respect to the reference period in Figures 9a, 9b, 9d and 9e; and differences between NOAH and SLAB in the changes expressed in percentage in Figures 9c and 9f. Solid contours are positive, dashed contours are negative, and dotted contours represent zero-isolines. Contour interval is 20.

NOAH scheme is used (Figures 10c and 11c). That is, the NOAH scheme provides larger (smaller) negative (positive) signals for the non-convective (convective) precipitation than the SLAB scheme.

[31] Figures 10d, 10e, 10g, and 10h (11d, 11e, 11g, and 11h) show the projected changes in frequency and intensity for the convective (non-convective) precipitation events, defined as the number of days per season with precipitation over 0.1 mm and the mean amount of precipitation per rainy day, respectively. The positive (negative) signals described above are accompanied by increases (decreases) in both the intensity and frequency of the rainy days without great controversy, i.e. if frequency decreases, intensity decreases, and vice versa, at least over the areas where changes are significant. This is common for both convective and non-convective precipitation, and occurs in both NOAH and SLAB simulations.

[32] To compare the relative importance of both contributions (i.e. the intensity and frequency of rainy days) to the changes in convective and non-convective precipitation, we computed separately the change that would result if only the frequency changed (i.e. keeping the intensity constant), and the change that would result if only the intensity changed (i.e. keeping the frequency constant). The black points in Figures 10d, 10e, 10g, 10h, 11d, 11e, 11g, and 11h show in which areas each contribution is more important than the other, and the gray points where they have opposite signs. This assessment does not reveal qualitative differences between the SLAB and the NOAH experiments, but does highlight some interesting features. The negative signals for non-convective precipitation are mainly due to the

reduction in the amount of precipitation when it falls, while the negative signals for convective precipitation are mainly due to the reduction in the number of days with convective precipitation events. However, the positive signals found for the convective precipitation are related to increases in the intensity rather than in the frequency.

[33] These features allow us to speculate that soil water recycling occurs over the IP. Although the general behavior is imposed by the synoptic forcing, and thus appears similar in both experiments, there are important differences between the two experiments regarding the intensity of the signals, where the LSM plays its major role. Given that soil moisture availability decreases when NOAH is used, it was to be expected (under the former assumption) that the NOAH simulation projects a larger reduction in the intensity of the non-convective rainy days and a smaller increase in the intensity of the convective rainy days than the SLAB simulation.

[34] Nevertheless, although it has been reported that the effect of the locally evaporated moisture added to the imported moisture from outer regions may be important, even crucial, in generating precipitation [*Schär et al.*, 1999], it is difficult to establish the concrete underlying mechanisms driving the differences found between the SLAB and the NOAH experiments. Feedbacks between soil moisture and precipitation have been analyzed in works such as those by *Barros and Hwu* [2002], *Luo et al.* [2007] and *Alfieri et al.* [2008], but it is still unclear whether, how, and under what circumstances these interactions influence precipitation forecasts. This assessment further reveals the complexity of the processes through which soil moisture
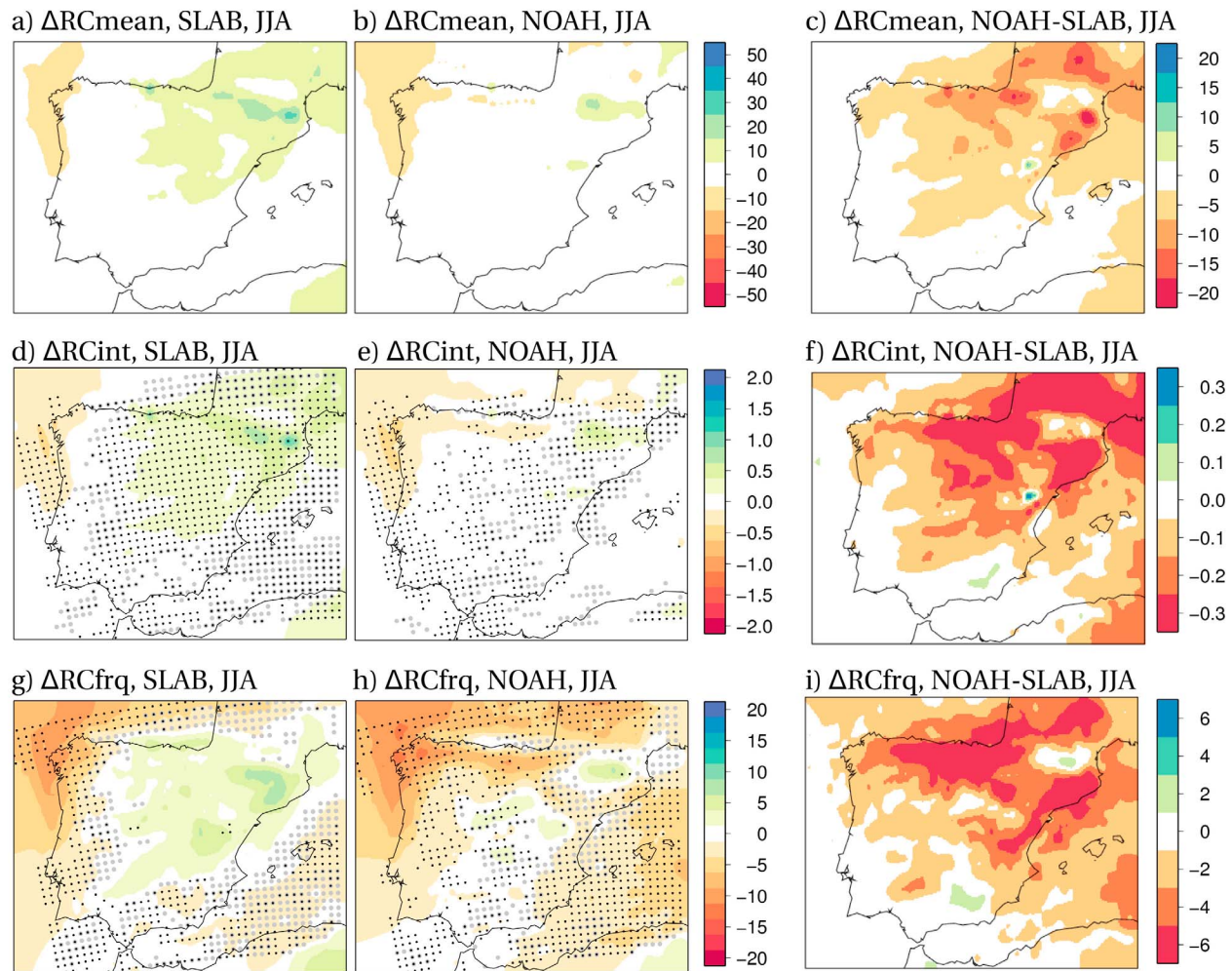
Figure 10. Changes in the summer (JJA) mean convective precipitation (RC) using either (a) the SLAB or (b) the NOAH scheme. (c) The differences between both projections (NOAH minus SLAB). Units: mm/month. Analogously, (d and e) changes in the intensity and (g and h) frequency of the RC events occurring at summertime using either the SLAB or the NOAH scheme. (f and i) Differences between both projections. Units: mm/day considering only rainy days for the intensity, and number of rainy days per year for the frequency. Black points mean that the change in the intensity (frequency) would produce alone a large change signal than the change in the frequency (intensity) alone. Gray points indicate where the change signals for intensity and frequency of the RC events have opposite sign.

and other soil variables and processes influence precipitation: we found no direct relations between the spatial distribution of patterns (although some of the more interesting signals tended to appear over the northern IP, which is the one considered as a transitional climate zone), or between the temporal evolution of series. In addition, important signals were observed in the LSM-impact patterns over the sea, where, necessarily, the influence of the LSM manifests indirectly. Nonetheless, the above results emphasize the strong influence of the land surface model when projecting future changes of precipitation over the IP, both directly and indirectly (via its influence on the simulated circulation, temperature, etc.) and perhaps through both positive and negative feedback processes. Likely, through a mix of all of these possibilities, which prevents a direct attribution as in the case of temperature. Such an influence mainly involves

the intensity of the changes, while patterns depict similar structures without depending on the LSM.

3.3. Changes in the Regional Circulation

[35] It is to be expected that differences in the surface energy balance between NOAH and SLAB simulations will also influence future projections for regional circulations, and that differences in regional circulations will contribute reciprocally to the differences in precipitation and temperature described above.

[36] Figures 12a, 12b, 12d, and 12e show the projected changes for 10-m wind and sea level pressure (SLP) for the winter and summer seasons in both simulations. In winter, the changes indicate a decrease in zonal winds related to the latitudinal increase in SLP. The intensification of the easterly winds appears similar in both experiments (Figure 12c), and thus it should be an issue derived basically from the
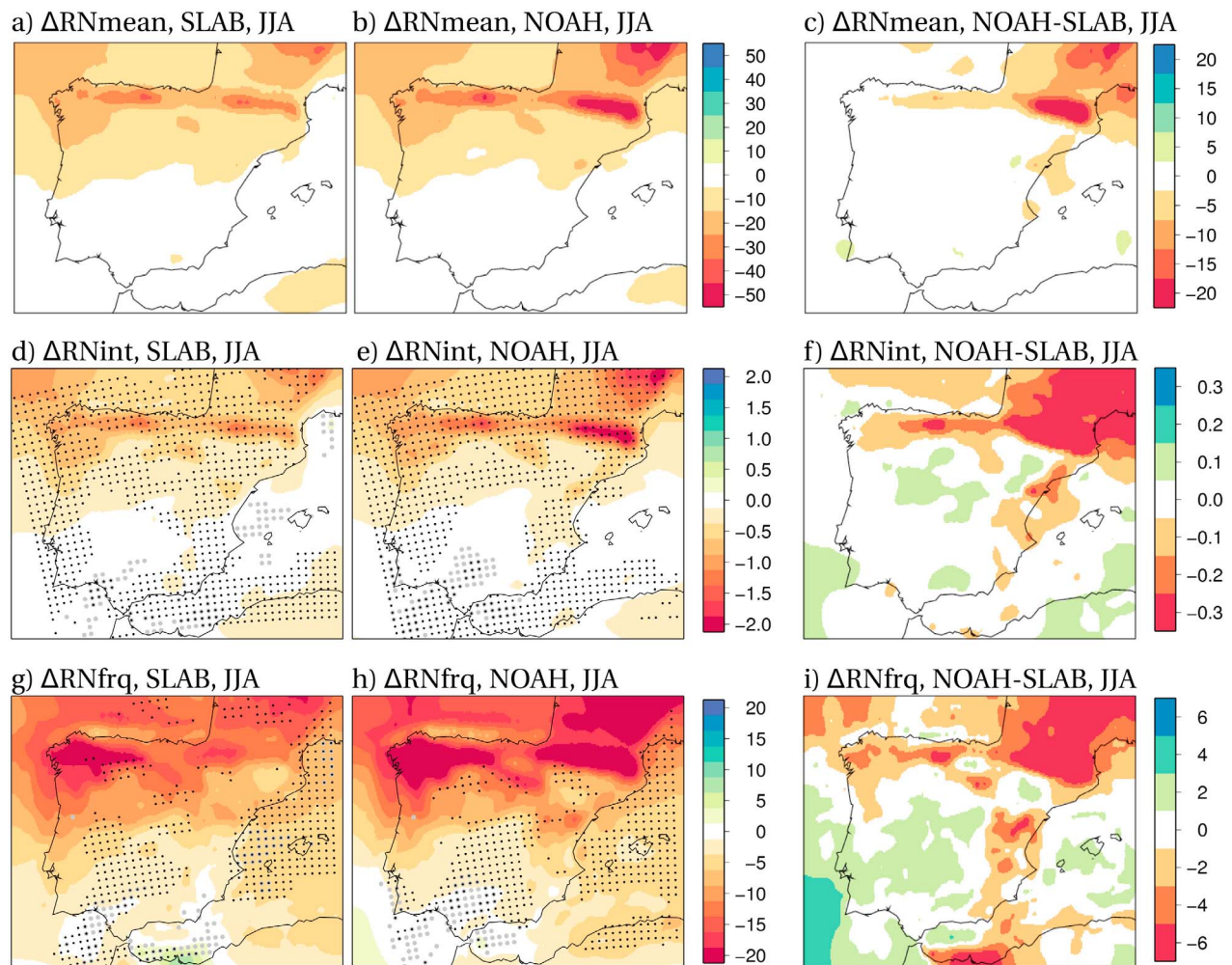
Figure 11. Same as Figure 10 but for non-convective precipitation (RN).

boundary conditions. The projected changes during summer also point to an intensification of the easterly winds in both simulations. This agrees with the idea proposed by *Haarsma et al.* [2009] that the drier Mediterranean soils intensify easterly winds. The differences between both experiments during summer (Figure 12f) point to an enhancement of the Iberian thermal low [*Hoinka and Castro*, 2003] in the NOAH simulation. This leads to a stronger cyclonic circulation around the IP and reveals that the LSM-impact during summer mainly affects the meso-alpha scale of motion. The enhancement of the thermal low is associated with the drier soils simulated by NOAH that lead to an increase of the sensible heat flux (Figure 5).
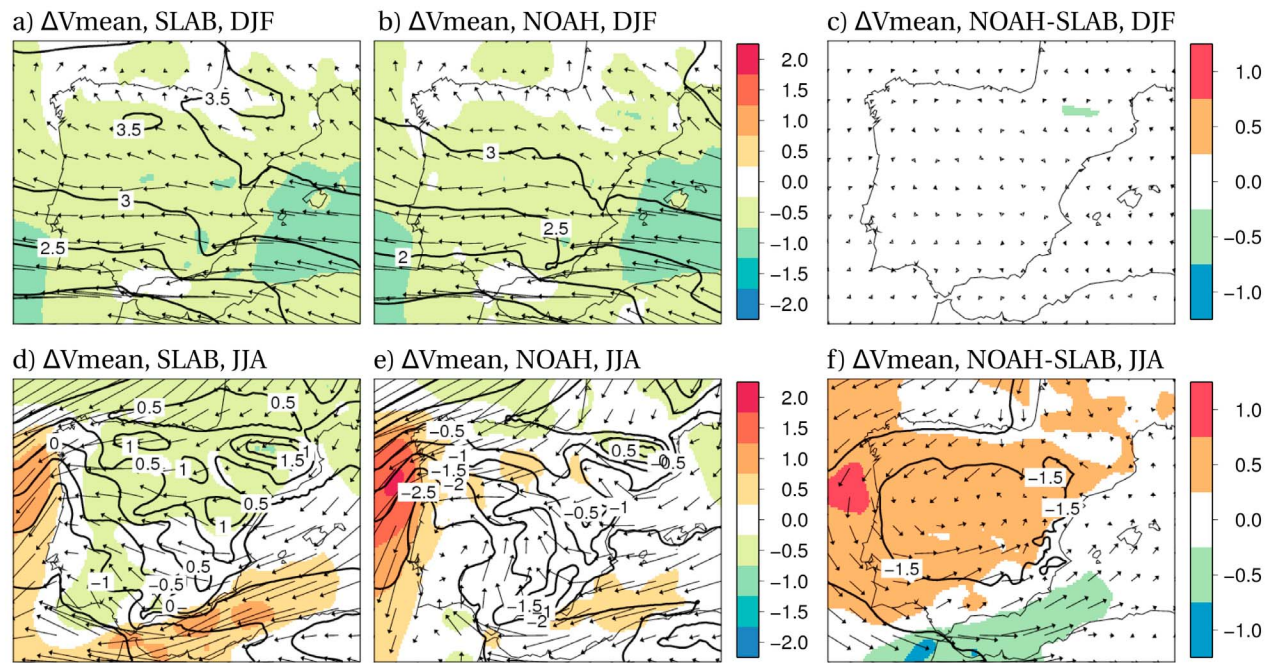
[37] Changes in the standard deviation of the surface wind speed and the SLP are shown in Figure 13. There is a reduction in both the wind speed and SLP variability during winter (Figures 13a and 13b), which seems to be associated with the higher SLPs simulated by both LSMs (Figures 12a and 12b), indicating a reinforcement of the Azores high pressure and its blocking of the westerly circulations. The differences between both projections (Figure 13c) point to a larger variability in the NOAH projection. During summer (Figures 13d and 13e), changes in variability are much more moderate than during winter. The differences between both

projections highlight the effects of the reinforcement of the Iberian thermal low by NOAH (Figure 13f). In particular, an increase in SLP variability over the center of the IP can be recognized.
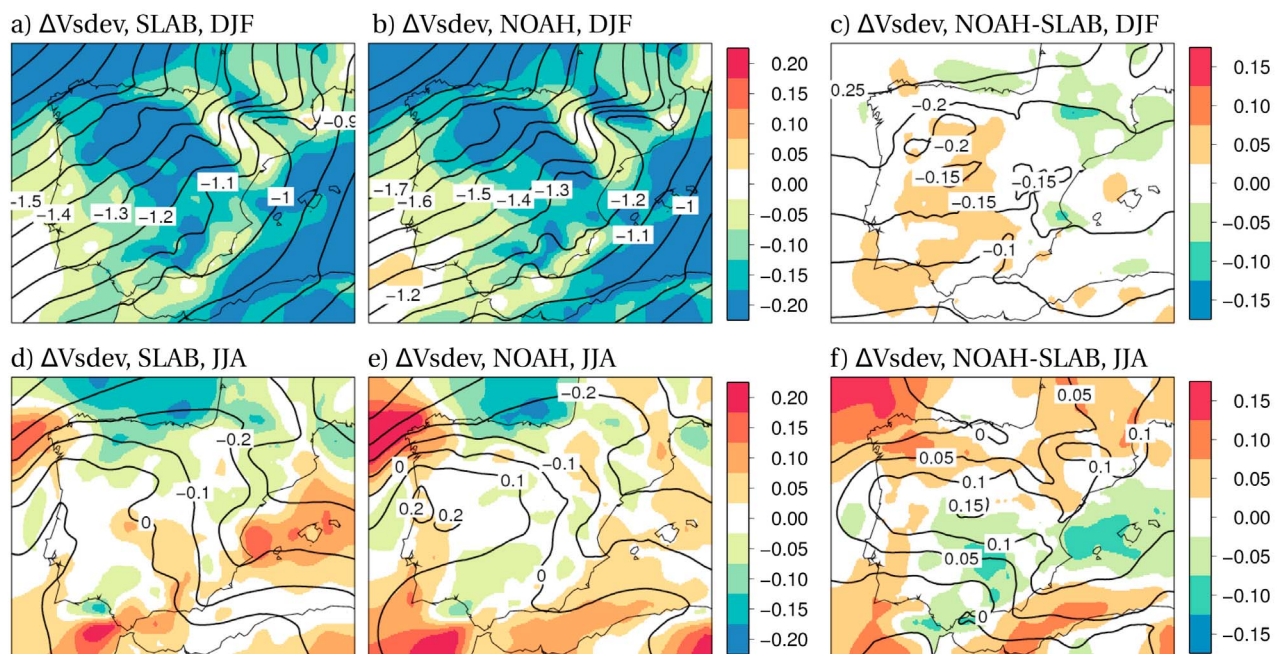
4. Summary and Conclusions

[38] This work assesses regional climate change projections for the Iberian Peninsula aimed at elucidating both the main signals and the role of the LSM, i.e. the influence of soil processes. Attention has particularly been paid to temperature and precipitation, although changes in surface wind are also analyzed. The evaluation focuses on mean values and interannual variability for the winter and summer seasons. Two LSMs available within the mesoscale model MM5, the simple SLAB model and the more complex NOAH scheme, have been used in this work. The main conceptual difference between them lies in the treatment of soil moisture, which is either fixed and given by the land use categorization or dynamically modeled, respectively.

[39] The regional climate change projections for temperature are characterized by an increase in both mean temperature and temperature variability, especially in the summer season (up to 6 K and over 40%, respectively). In addition,

a) ΔVmean, SLAB, DJF

b) ΔVmean, NOAH, DJF

c) ΔVmean, NOAH-SLAB, DJF

d) ΔVmean, SLAB, JJA

e) ΔVmean, NOAH, JJA

f) ΔVmean, NOAH-SLAB, JJA

Figure 12. (a, b, d, and e) Projections for the mean module of the surface wind (Vmean, by shaded colors) and for the mean sea level pressure (SLP, by contours), using either the SLAB or the NOAH scheme, for the winter (DJF) and summer (JJA) seasons. (c and f) The differences between the NOAH and the SLAB projection. Units: V in m/s and SLP in hPa (contour interval is 0.5 hPa). Arrows represent changes in the wind vector at 10 m height.

a) ΔVsdev, SLAB, DJF

b) ΔVsdev, NOAH, DJF

c) ΔVsdev, NOAH-SLAB, DJF

d) ΔVsdev, SLAB, JJA

e) ΔVsdev, NOAH, JJA

f) ΔVsdev, NOAH-SLAB, JJA

Figure 13. (a, b, d, and e) Projections for the interannual variability of the module of the surface wind (Vsdev, by shaded colors) and for the sea level pressure (SLP, by contours), using either the SLAB or the NOAH scheme, for the winter (DJF) and summer (JJA) seasons. (c and f) The differences between the NOAH and the SLAB projection. Units: V in m/s and SLP in hPa. Contour interval is 0.1 hPa (in Figures 13a, 13b, 13d, and 13e) and 0.05 hPa (in Figures 13c and 13f).

precipitation is projected to decrease by around 40% in both winter and summer seasons [*Perez et al.*, 2010]. This signal results from a reduction in both the intensity and frequency of both convective and non-convective precipitation events. The exception is that the summertime convective precipitation is projected to increase, due to further intensification of the convective rainfall events rather than to an increase in the number of this kind of event. The surface wind circulations show a weakening of the predominant westerly winds.

[40] The strongest influence of the soil forcing on the above projections was found for the summer season. Large scale circulation tightly controls temperature, precipitation and winds in wintertime, while in summer the synoptic scale winds are weaker and thus local circulations become more relevant in midlatitude regions, such as the IP [*Font-Tullot*, 2000]. Moreover, solar forcing is weaker in winter than in summer and therefore less heat is available for its partitioning into sensible and latent fluxes. Both features prevent a strong influence of in-situ processes, such as soil-atmosphere feedbacks, in the winter season, while increasing the importance of the LSM in the summer season.

[41] The future intensification of the positive soil moisture-atmosphere feedback [*Jerez et al.*, 2010] strengthens the future warming projected. The areas where land-surface coupling amplifies the projected warming lie in the driest inner areas of the IP, where the use of the NOAH scheme favors the exchange of sensible heat between the land and the atmosphere at the expense of the latent heat in comparison with the SLAB simulation. Moreover, it reveals a future amplification of the daily temperature range, since maximum temperatures are more sensitive to such sensible heat exchange than minima. This feature is totally masked when using the simplest soil model treating soil moisture as a static field. Conversely, the LSM plays a greater role in the wetter northern IP as regards temperature variability projections. These areas are those where the reduction in the soil moisture content is more dramatic, a feature that turns them into semi-arid regimes (hence they are called transitional climate zones [*Seneviratne et al.*, 2006b]) and enhances the projected increases.

[42] Assessment of the precipitation projections reveals that the use of the more complex NOAH LSM provides stronger negative signals for non-convective precipitation and smaller positive signals for convective precipitation. However, it is difficult to establish a direct link with the soil moisture forcing in this case. Feedback between soil moisture and precipitation can occur both directly, i.e. through the recycling of water [*Schär et al.*, 1999], and indirectly, e.g. through impacts on temperature and regional circulations [*Jimenez et al.*, 2011]. In fact, some of the largest differences between both analyzed simulations appeared over the sea, where they necessarily come indirectly from the soil forcing, whatever it was.

[43] Regarding changes in regional circulation, the NOAH projection shows a deeper reinforcement of the Iberian thermal low than the simpler SLAB scheme. As a consequence, NOAH shows higher cyclonic mesoscale circulations over the IP. The reinforcement of the Iberian low is related to the increase in the sensible heat flux in NOAH due to the drier soils projected in the future. This modeling study therefore reveals that modifications in the available soil moisture are able to modify the surface wind in regional climate change projections through the meso-gama scales of motion [*Jimenez et al.*, 2011].

[44] Although the patterns usually depict similar structures with no dependence on the LSM, the results indicate that the soil forcing can strongly modify the intensity of the projected changes. Therefore, the reliability of the LSM seems essential for properly evaluating future climate change-derived risks and extreme events [*Seneviratne et al.*, 2006b; *Fischer et al.*, 2007; *Fischer and Schär*, 2009]. Land-surface parameters such as the vegetation fraction that largely determines the way in which soil administers the available water and which are, however, poorly represented in climate simulation models and usually treated as a static field, may deserve further attention to increase accuracy [*Pielke*, 2001; *Kato et al.*, 2007]. In general, a deeper understanding of land-atmosphere feedbacks is strongly desirable in this regard [*Seneviratne et al.*, 2010].

[45] Furthermore, a cascade on uncertainties can be intuited given the paramount importance of the soil forcing. For instance, the uncertainties associated with the precipitation projections [*Perez et al.*, 2010] translates directly into uncertainties regarding soil moisture availability. Therefore, temperature and wind projections would also be affected by this additional uncertainty derived from (or induced by) the uncertainty associated with the simulated soil moisture content.

References

Alfieri, L., P. Claps, P. D'Odorico, F. Laio, and T. M. Over (2008), An analysis of the soil moisture feedback on convective and stratiform precipitation, *J. Hydrometeorol.*, *9*(2), 280–291.

Barros, A. P., and W. J. Hwu (2002), A study of land-atmosphere interactions during summertime rainfall using a mesoscale model, *J. Geophys. Res.*, *107*(D14), 4227, doi:10.1029/2000JD000254.

Betts, A. K. (2004), Understanding hydrometeorology using global models, *Bull. Am. Meteorol. Soc.*, *85*(11), 1673–1688.

Chen, F., and J. Dudhia (2001), Coupling an advanced land surface-hydrology model with the Penn State-NCAR MM5 modeling system. Part I: Model implementation and sensitivity, *Mon. Weather Rev.*, *129*(4), 569–585.

Christensen, J. H., and O. B. Christensen (2007), A summary of the PRUDENCE model projections of changes in European climate by the end of this century, *Clim. Change*, *81*, 7–30.

Della-Marta, P. M., M. R. Haylock, J. Luterbacher, and H. Wanner (2007), Doubled length of western European summer heat waves since 1880, *J. Geophys. Res.*, *112*, D15103, doi:10.1029/2007JD008510.

Dirmeyer, P. A., X. Gao, M. Zhao, Z. Guo, T. Oki, and N. Hanasaki (2006), GSWP-2: Multimodel analysis and implications for our perception of the land surface, *Bull. Am. Meteorol. Soc.*, *87*, 1381–1397.

Dudhia, J. (1989), Numerical study of convection observed during the winter monsoon experiment using a mesoscale two-dimensional model, *J. Atmos. Sci.*, *46*(20), 3077–3107.

Dudhia, J. (1996), A multi-layer soil-temperature model for MM5, paper presented at Sixth PSU/NCAR MMU Workshop, Natl. Cent. for Atmos. Res., Boulder, Colo.

Fernandez, J., J. P. Montavez, J. Saenz, J. F. Gonzalez-Rouco, and E. Zorita (2007), Sensitivity of the MM5 mesoscale model to physical parameterizations for regional climate studies: Annual cycle, *J. Geophys. Res.*, *112*, D04101, doi:10.1029/2005JD006649.

Ferranti, L., and P. Viterbo (2006), The European summer of 2003: Sensitivity to soil water initial conditions, *J. Clim.*, *19*(15), 3659–3680.

Fischer, E. M., and C. Schär (2009), Future changes in daily summer temperature variability: Driving processes and role for temperature extremes, *Clim. Dyn.*, *33*, 917–935.

Fischer, E. M., S. I. Seneviratne, P. L. Vidale, D. Lüthi, and C. Schär (2007), Soil moisture-atmosphere interactions during the 2003 European summer heatwave, *J. Clim.*, *20*, 5081–5099.

Font-Tullot, I. (2000), *Climatologia de España y Portugal*, Univ. de Salamanca, Salamanca, Spain.

Gallardo, C., A. Arribas, J. A. Prego, M. A. Gaertner, and M. de Castro (2001), Multi-year simulations using a regional-climate model over the Iberian Peninsula: current climate and doubled CO_2 scenario, *Q. J. R. Meteorol. Soc.*, *127*, 1659–1681.

Gao, X., and F. Giorgi (2008), Increased aridity in the Mediterranean region under greenhouse gas forcing estimated from high resolution simulations with a regional climate model, *Global Planet. Change*, *62*, 195–209.

Giorgi, F. (2006), Climate change hot-spots, *Geophys. Res. Lett.*, *33*, L08707, doi:10.1029/2006GL025734.

Gomez-Navarro, J. J., J. P. Montavez, P. Jimenez-Guerrero, S. Jerez, J. A. Garcia-Valero, and J. F. Gonzalez-Rouco (2010), Warming patterns in regional climate change projections over the Iberian Peninsula, *Meteorol. Z.*, *19*(3), 275–285.

Gomez-Navarro, J. J., J. P. Montavez, S. Jerez, P. Jimenez-Guerrero, R. Lorente-Plazas, J. F. Gonzalez-Rouco, and E. Zorita (2011), A regional climate simulation over the Iberian Peninsula for the last millennium, *Clim. Past*, *7*, 451–472.

Gonzalez-Rouco, J. F., H. Heyen, E. Zorita, and F. Valero (2000), Agreement between observed rainfall trends and climate change simulations in the southwest of Europe, *J. Clim.*, *13*, 3057–3065.

Grell, G. A. (1993), Prognostic evaluation of assumptions used by cumulus parameterizations, *Mon. Weather Rev.*, *121*(3), 764–787.

Grell, G. A., J. Dudhia, and D. R. Stauffer (1994), A description of the fifth-generation Penn State/NCAR Mesoscale Model (MM5), *NCAR Tech. Note 398+STR*, 117 pp., Natl. Cent. for Atmos. Res., Boulder, Colo.

Gulden, L. E., E. Rosero, Z. L. Yang, T. Wagener, and G. Y. Niu (2008), Model performance, model robustness, and model fitness scores: A new method for identifying good land-surface models, *Geophys. Res. Lett.*, *35*, L11404, doi:10.1029/2008GL033721.

Guo, Z. C., et al. (2006), The Global Land-Atmosphere Coupling Experiment. Part II: Analysis, *J. Hydrometeorol.*, *7*, 611–625.

Haarsma, R. J., F. Selten, B. vd Hurk, W. Hazeleger, and X. Wang (2009), Drier Mediterranean soils due to greenhouse warming bring easterly winds over summertime central Europe, *Geophys. Res. Lett.*, *36*, L04705, doi:10.1029/2008GL036617.

Henderson-Sellers, A., K. McGuffie, and A. Pitman (1996), The Project for Intercomparison of Land-Surface Parametrization Schemes (PILPS): 1992 to 1995, *Clim. Dyn.*, *12*, 849–859.

Hohenegger, C., P. Brockhaus, C. Bretherton, and C. Schär (2008), The soil moisture-precipitation feedback in simulations with explicit and parameterized convection, *J. Clim.*, *22*(19), 5003–5020.

Hoinka, K. P., and M. D. E. Castro (2003), The Iberian Peninsula thermal low, *Q. J. R. Meteorol. Soc.*, *129*(590), 1491–1511.

Hong, S.-Y., and H.-L. Pan (1996), Nonlocal boundary layer vertical diffusion in a medium-range forecast model, *Mon. Weather Rev.*, *124*, 2322–2339.

Jaeger, E. B., and S. I. Seneviratne (2010), Impact of soil moisture-atmosphere coupling on European climate extremes and trends in a regional climate model, *Clim. Dyn.*, *36*(9), 1919–1939.

Jaeger, E. B., R. Stöckli, and S. I. Seneviratne (2009), Analysis of planetary boundary layer fluxes and land-atmosphere coupling in the regional climate model CLM, *J. Geophys. Res.*, *114*, D17106, doi:10.1029/2008JD011658.

Jerez, S., J. P. Montavez, J. J. Gomez-Navarro, P. Jimenez-Guerrero, J. Jimenez, and J. F. Gonzalez-Rouco (2010), Temperature sensitivity to the land-surface model in MM5 climate simulations over the Iberian Peninsula, *Meteorol. Z.*, *19*(4), 363–374.

Jimenez, P. A., J. Vila-Guerau de Arellano, J. F. Gonzalez-Rouco, J. Navarro, J. P. Montavez, E. Garcia-Bustamante, and J. Dudhia (2011), The effect of heatwaves and drought on surface wind circulations in the NE of the Iberian Peninsula during the summer of 2003, *J. Clim.*, *24*, 5416–5422.

Jimenez-Guerrero, P., J. J. Gomez-Navarro, R. Lorente, S. Jerez, J. A. Garcia-Valero, and J. P. Montavez (2010), Variation of Secondary Inorganic Aerosols (SIA) in Europe for the 21st century (1991–2100), *Atmos. Environ.*, *45*(4), 1059–1063.

Kanamitsu, M., W. Ebisuzaki, J. Woollen, S.-K. Yang, J. J. Hnilo, M. Fiorino, and G. L. Potter (2002), NCEP-DOE AMIP-II Reanalysis (R-2), *Bull. Am. Meteorol. Soc.*, *83*, 1631–1643.

Kato, H., M. Rodell, F. Beyrich, H. Cleugh, E. van Gorsel, H. Liu, and T. P. Meyers (2007), Sensitivity of land surface simulations to model physics, land characteristics, and forcings, at four CEOP sites, *J. Meteorol. Soc. Japan*, *85*(0), 187–204.

Koo, G. S., K. O. Boo, and W. T. Kwon (2009), Projection of temperature over Korea using an MM5 regional climate simulation, *Clim. Res.*, *40*(2–3), 241–248.

Koster, R. D., and M. J. Suarez (2001), Soil moisture memory in climate models, *J. Hydrometeorol.*, *2*(6), 558–570.

Koster, R. D., et al. (2004), Regions of strong coupling between soil moisture and precipitation, *Science*, *305*, 1138–1140.

Koster, R. D., et al. (2006), GLACE: The Global Land-Atmosphere Coupling Experiment. Part I: Overview, *J. Hydrometeorol.*, *7*, 590–610.

Legutke, S., and R. Voss (1999), ECHO-G, The Hamburg Atmosphere–Ocean Coupled Circulation Model, *Dtsch. Klimarechenzent.*, *18*, 43 pp.

Luo, Y., E. H. Berbery, K. E. Mitchell, and A. K. Betts (2007), Relationships between land surface and near-surface atmospheric variables in the NCEP North American Regional Reanalysis, *J. Hydrometeorol.*, *8*(6), 1184–1203.

Manabe, S. (1969), Climate and ocean circulation. I. Atmospheric circulation and hydrology of Earth's surface, *Mon. Weather Rev.*, *97*, 739–774.

May, W. (2008), Potential future changes in the characteristics of daily precipitation in Europe simulated by the HIRHAM regional climate model, *Clim. Dyn.*, *30*, 581–603.

Miao, J. F., D. Chen, and K. Borne (2007), Evaluation and comparison of Noah and Pleim-Xiu land surface models in MM5 using GÖTE2001 data: Spatial and temporal variations in near-surface air temperature, *J. Appl. Meteorol. Climatol.*, *46*(10), 1587–1605.

Mlawer, E. J., S. J. Taubman, P. D. Brown, M. J. Iacono, and S. A. Clough (1997), Radiative transfer for inhomogeneous atmospheres: RRTM, a validated correlated-k model for the longwave, *J. Geophys. Res.*, *102*, 16,663–16,682, doi:10.1029/97JD00237.

Perez, F. F., et al. (2010), Clima en España: Pasado, presente y futuro: Informe de Evaluacion del Cambio Climatico Regional, report, Span. Min. of Sci. and Innovation, Madrid, Spain.

Pielke, R. A., Sr. (2001), Influence of the spatial distribution of vegetation and soils on the prediction of cumulus convective rainfall, *Rev. Geophys.*, *39*(2), 151–177, doi:10.1029/1999RG000072.

Pitman, A. (2003), The evolution of, and revolution in, land surface schemes designed for climate models, *Int. J. Clim.*, *23*, 479–510.

Pitman, A., et al. (2009), Uncertainties in climate responses to past land cover change: First results from the LUCID intercomparison study, *Geophys. Res. Lett.*, *36*, L14814, doi:10.1029/2009GL039076.

Robock, A., K. Y. Vinnikov, G. Srinivasan, J. K. Entin, S. E. Hollinger, N. A. Speranskaya, S. Liu, and A. Namkhai (2000), The global soil moisture data bank, *Bull. Am. Meteorol. Soc.*, *81*(6), 1281–1299.

Schär, C., D. Lüthi, U. Beyerle, and E. Heise (1999), The soil-precipitation feedback: A process study with a regional climate model, *J. Clim.*, *12*(3), 722–741.

Seneviratne, S. I., et al. (2006a), Soil moisture memory in AGCM mimulations: Analysis of Global Land–Atmosphere Coupling Experiment (GLACE) data, *J. Hydrometeorol.*, *7*(5), 1090–1112.

Seneviratne, S. I., D. Luethi, M. Litschi, and C. Schaer (2006b), Land-atmosphere coupling and climate change in Europe, *Nature*, *443*(7108), 205–209.

Seneviratne, S. I., T. Corti, E. L. Davin, M. Hirschi, E. B. Jaeger, I. Lehner, B. Orlowsky, and A. J. Teuling (2010), Investigating soil moisture-climate interactions in a changing climate: A review, *Earth Sci. Rev.*, *99*(3–4), 125–161.

Sridhar, V., R. L. Elliott, F. Chen, and J. A. Brotzge (2002), Validation of the NOAH-OSU land surface model using surface flux measurements in Oklahoma, *J. Geophys. Res.*, *107*(D20), 4418, doi:10.1029/2001JD001306.

Steiner, A. L., J. S. Pal, S. A. Rauscher, J. L. Bell, N. S. Diffenbaugh, A. Boone, L. C. Sloan, and F. Giorgi (2009), Land surface coupling in regional climate simulations of the West African monsoon, *Clim. Dyn.*, *33*(6), 869–892.

Sumner, G. N., R. Romero, V. Homar, C. Ramis, S. Alonso, and E. Zorita (1995), An estimate of the effects of climate change on the rainfall of Mediterranean Spain by the late twenty first century, *Int. J. Clim.*, *15*, 673–696.

Tapiador, F. J., E. Sanchez, and M. A. Gaertner (2007), Regional changes in precipitation in Europe under an increased greenhouse emissions scenario, *Geophys. Res. Lett.*, *34*, L06701, doi:10.1029/2006GL029035.

Taylor, C. M., D. J. Parker, and P. P. Harris (2007), An observational case study of mesoscale atmospheric circulations induced by soil moisture, *Geophys. Res. Lett.*, *34*, L15801, doi:10.1029/2007GL030572.

Trigo, R. M., and J. P. Palutikof (2001), Precipitation scenarios over Iberia: A comparison between direct GCM output and different downscaling techniques, *J. Clim.*, *14*, 4422–4446.

Yang, S., S. H. Yoo, R. Yang, K. E. Mitchell, H. van den Dool, and R. W. Higgins (2007), Response of seasonal simulations of a regional climate model to high-frequency variability of soil moisture during the summers of 1988 and 1993, *J. Hydrometeorol.*, *8*(4), 738–757.

Zhang, J., W. C. Wang, and J. Wei (2008), Assessing land-atmosphere coupling using soil moisture from the Global Land Data Assimilation System and observational precipitation, *J. Geophys. Res.*, *113*, D17119, doi:10.1029/2008JD009807.

Zhang, J., W. C. Wang, and L. Wu (2009), Land-atmosphere coupling and diurnal temperature range over the contiguous United States, *Geophys. Res. Lett.*, *36*, L06706, doi:10.1029/2009GL037505.

Zorita, E., J. F. González-Rouco, H. von Storch, J. P. Montávez, and F. Valero (2005), Natural and anthropogenic modes of surface temperature variations in the last thousand years, *Geophys. Res. Lett.*, *32*, L08707, doi:10.1029/2004GL021563.

J. J. Gomez-Navarro, S. Jerez, P. Jimenez-Guerrero, R. Lorente, and J. P. Montavez, Departamento de Fisica, Universidad de Murcia, Campus de Espinardo, Edificio CIOyN, E-30100 Murcia, Spain. (jjgomeznavarro@um.es; sonia.jerez@gmail.com; pedro.jimenezguerrero@um.es; lorente.plazas@gmail.com; montavez@um.es)

J. F. Gonzalez-Rouco, Departamento Astrofisica y Ciencias de la Atmosfera, Facultad Ciencias Fisicas, Universidad Complutense de Madrid, E-28040 Madrid, Spain. (fidelgr@fis.ucm.es)

P. A. Jimenez, National Center for Atmospheric Research, Boulder, CO 80307, USA. (pedro.jimenez@fis.ucm.es)